Letter

Possible quantization and half-quantization in the anomalous Hall effect caused by in-plane magnetic field

Song Sun,[1,2] Hongming Weng,[1,2,3] and Xi Dai[4,5,*]

[1]*Beijing National Laboratory for Condensed Matter Physics, and Institute of Physics, Chinese Academy of Sciences, Beijing 100190, China*
[2]*University of Chinese Academy of Sciences, Beijing 100049, China*
[3]*Songshan Lake Materials Laboratory, Dongguan, Guangdong 523808, China*
[4]*Department of Physics, Hong Kong University of Science and Technology, Clear Water Bay, Hong Kong*
[5]*Materials Department, University of California, Santa Barbara, California 93106-5050, USA*

(Received 4 April 2022; revised 7 August 2022; accepted 22 November 2022; published 14 December 2022)

In this paper we propose that quantized and nearly half-quantized intrinsic anomalous Hall effect can be induced by in-plane external magnetic field through the Zeeman coupling in nonmagnetic two-dimensional (2D) systems with sizable spin-orbital coupling but without twofold rotational symmetry. An analytical result is derived for the 2D electron gas model with C_{3v} symmetry. Further, based on the $\boldsymbol{k}\cdot\boldsymbol{p}$ Hamiltonian derived from first principle calculations, we find that the quantized and nearly half-quantized Hall conductance can be observed in Sb_2Te_3 thin film in the clean limit with strong in-plane magnetic field $B > 20$ T and low temperature $T < 100$ mK.

DOI: 10.1103/PhysRevB.106.L241105

Introduction. The Hall effect, where the transverse voltage is induced by the longitudinal current, is one of the fundamental effects for metallic systems. It contains both the ordinary and anomalous parts of contribution, where the former is caused by the Lorentz force under an external magnetic field and the latter is due to the spin-orbital effect in systems with magnetic order that breaks time reversal symmetry. The anomalous contribution to the Hall effect is called the anomalous Hall effect (AHE), which can be further divided into intrinsic and extrinsic mechanisms [1]. For the intrinsic mechanism, when an electric current is passing though the sample, the Bloch electrons acquire an additional anomalous velocity [2] along the perpendicular direction, which causes the Hall current. Such a mechanism is an intrinsic property of the Bloch states in a perfect crystal without time reversal symmetry. In contrast, the extrinsic mechanism originates from the scattering from disorder.

Among these contributions, the intrinsic AHE has received great attention [3–6] in these years because it is one of the intrinsic properties for band structure of crystal, which can be obtained by integrating the Berry curvature over all the occupied Bloch states. The intrinsic AHE conductance in two dimensions can be obtained as [1]

$$\sigma_{xy} = -\frac{e^2}{h}\sum_n \int \frac{d^2\boldsymbol{k}}{2\pi} f(\epsilon_n(\boldsymbol{k}))b_n(\boldsymbol{k}), \tag{1}$$

where $b_n(\boldsymbol{k})$ is the Berry curvature of the nth band and $f(\epsilon_n(\boldsymbol{k}))$ is the Fermi-Dirac distribution function. For systems with time reversal symmetry $\mathcal{T}$, the net contribution described by Eq. (1) has to be zero, because the Berry curvature contributed by each particular Bloch state $|n,\boldsymbol{k}\rangle$ will be exactly canceled by its time reversal partner $\mathcal{T}|n,\boldsymbol{k}\rangle$. In ferromagnetic metals, for which the AHE is mostly studied, the magnetization $\boldsymbol{M}$ breaks the time reversal symmetry and induces the net contribution to the Hall conductance. Moreover, the intrinsic AHE conductance can be possibly quantized to realize the quantum anomalous Hall effect (QAHE) [7] when the chemical potential lies in a band gap, and the resulting band structure can be characterized by a topological index called Chern number [8,9].

Besides the ferromagnetic metal, the AHE can also be found in nonmagnetic metals or semiconductors, where the time reversal symmetry is broken not by spontaneous magnetization but the Zeeman effect caused by an external magnetic field [10,11]. When the field is applied along the z direction, the Zeeman effect is always coexisting with the Lorentz force or its quantum version, the Landau quantization, which makes it difficult to distinguish the two types of contributions. However, if we consider a two-dimensional (2D) system and apply the field within the xy plane, the Lorentz force or Landau quantization will not exist and the Hall conductance detected in such a case (if any) will be completely caused by the Zeeman effect.

In the present paper, we will focus on such an in-plane AHE caused by the Zeeman effect which has not received the attention it deserves. Based on the symmetry analysis, we first conclude that this in-plane AHE is ubiquitous in 2D metallic systems without twofold rotational symmetry C_{2z} [12,13]. Additionally, this in-plane AHE is more likely to be observed in systems with strong spin-orbit coupling (SOC), in which the Zeeman effect may be significantly enhanced in magnitude over free electrons [14,15]. Like the AHE in magnetic semiconductors, the in-plane AHE can also be quantized if the in-plane Zeeman effect opens a gap for the system or be nearly

*daix@ust.hk

half quantized if the main Berry curvature contribution of a single massive Dirac point is isolated with electric field and in-plane Zeeman field. The in-plane magnetization induced QAHE has been first discussed by Liu's group in magnetic topological insulator (TI) thin films [16]; however, studies of in-plane magnetic field induced sizable AHE, quantized AHE, and half-quantized AHE based on actual parameters (especially g factors) of materials are still lacking.

We will propose two typical 2D metallic or semimetallic systems to study this in-plane AHE. The first system is the 2D electron gas (2DEG) with strong SOC under point group symmetry C_{3v}. As we will introduce below, in such a system the SOC terms consist of both the linear Rashba term [17,18] and the cubic hexagonal warping term [19], which leads to large and nearly half-quantized in-plane AHE. This example establishes that in systems without C_{2z} symmetry the in-plane AHE emerges once the high order terms are taken into account. The second system discussed in detail will be the TI thin films. For these materials, we will first apply the first principle calculation to compute their g factors for the magnetic field using the method developed in our group [20], which indicates a very large in-plane Zeeman effect for the bulk material already. We then calculate the subband structure under the in-plane field for the Sb_2Te_3 thin film using the $\boldsymbol{k}\cdot\boldsymbol{p}$ model with its parameters being extracted from the first principle calculations, based on which the Hall conductance under the in-plane field can be obtained using Eq. (1). We demonstrate that for such a system by adjusting two different gates on both top and bottom surfaces both the quantized and nearly half-quantized in-plane AHE can be possibly reached under strong magnetic field and low temperature.

Nonmagnetic 2D electron gas. Nonzero in-plane AHE can only exist in systems without C_{2z} symmetry. The reason is that the in-plane magnetic field breaks both the C_{2z} and $\mathcal{T}$ but preserves the combination of them, namely $C_{2z}\mathcal{T}$ symmetry, and the Hall conductance changes sign under this $C_{2z}\mathcal{T}$ symmetry operation which makes it zero. Hence let us focus on the 2DEG with C_{3v} point group symmetry. The Hamiltonian of such a 2DEG can be written as

$$H=\frac{\hbar^2k^2}{2m}+\lambda(\boldsymbol{k}\times\boldsymbol{\sigma})\cdot\hat{z}+\frac{\delta}{2}(k_+^3+k_-^3)\sigma_z+\frac{\mu_B}{2}g\boldsymbol{\sigma}\cdot\boldsymbol{B}_\parallel, \tag{2}$$

where the first term is the kinetic term with m being the effective mass, the second term is the linear Rashba coupling, the third term is the generic hexagonal warping term which breaks the C_{2z} symmetry with $k_\pm=k_x\pm ik_y$, and the last term is the Zeeman coupling with μ_B being the Bohr magneton, g being the in-plane effective g factor, and $\boldsymbol{B}_\parallel$ being the in-plane magnetic field. The hexagonal warping term [19] breaks not only the continuous rotation symmetry in the z direction down to C_{3z} but also the vertical mirror symmetry from along all in-plane directions down to three discrete directions only. Since the vertical mirror symmetry also excludes the AHE [16], the external magnetic field has to be applied along the direction that breaks the mirror symmetry.

Any two band Hamiltonian can be decomposed by Pauli matrices as $H(\boldsymbol{k})=\epsilon(\boldsymbol{k})+\boldsymbol{d}(\boldsymbol{k})\cdot\boldsymbol{\sigma}$, with which the intrinsic AHE can be formulated in [21,22]

$$\sigma_{xy}=\int\frac{d^2\boldsymbol{k}}{4\pi}(f_+-f_-)\left(\partial_{k_x}\hat{\boldsymbol{d}}\times\partial_{k_y}\hat{\boldsymbol{d}}\right)\cdot\hat{\boldsymbol{d}}, \tag{3}$$

where $\hat{\boldsymbol{d}}(\boldsymbol{k})=\boldsymbol{d}(\boldsymbol{k})/d(\boldsymbol{k})$ is the normalized $\boldsymbol{d}$ vector and f_+ (f_-) is the Fermi-Dirac distribution function for the positive (negative) energy band. After some detailed calculation given in the Supplemental Material (SM) [22], we obtain that, when the chemical potential is large $\mu\gg E^*$ (E^* is the middle point of the Dirac gap), the leading term of the in-plane AHE conductance at the zero temperature limit is

$$\sigma_{xy}\approx-\frac{\delta\mu_B^3g^3B_\parallel^3}{16\mu\lambda^3}\sin 3\theta, \tag{4}$$

where θ is the angle between $\boldsymbol{B}_\parallel$ and $\hat{x}$. In contrast, when the chemical potential is tuned at the center of the Dirac gap $\mu=E^*$, the leading terms are

$$\sigma_{xy}\approx\begin{cases}-\frac{1}{2}\mathrm{sgn}(\sin 3\theta)+\frac{\delta\mu_B^2g^2B_\parallel^2}{16\lambda^3}\frac{\sin 3\theta}{\sqrt{1/\gamma^2-1}}, & \text{if } \gamma<1,\\ -\frac{1}{2\gamma}\mathrm{sgn}(\sin 3\theta), & \text{if } \gamma>1,\end{cases} \tag{5}$$

where $\gamma\equiv\frac{\hbar^2\mu_Bg B_\parallel}{2m\lambda^2}$ is a dimensionless quantity. When $\gamma\ll 1$, which is a common case for materials with large SOC constant λ under accessible field strength [23], the conductance approaches half-quantized value $\sigma_{xy}\to-\frac{1}{2}\mathrm{sgn}(\sin 3\theta)$. As shown in Figs. 1(a) and 1(b), numerical results are in good agreement with our analytical results in these limits. We also calculate the conductance versus the magnetic field strength with fixed electron density n at the zero temperature limit as shown in (c) and (d) and at 1 K temperature as shown in (e) and (f). Nearly half-quantized plateaus appear in (c) and (e).

The appearance of such a nearly half-quantized plateau in Hall conductance can be understood as follows. The Zeeman coupling caused by the in-plane field shifts the Dirac point away from the Γ point to $\boldsymbol{k}^*\equiv\frac{\mu_Bg}{2\lambda}(\hat{\boldsymbol{z}}\times\boldsymbol{B}_\parallel)$ [19], and the hexagonal warping term then opens a small gap $2\Delta^*\equiv 2\delta k^{*3}\sin 3\theta$ at the Dirac point and turns it into an anticrossing point as illustrated in the inset of Fig. 1(a). In the vicinity of the anticrossing point $\boldsymbol{k}^*$, the band structure can be described by a titled 2D Dirac model with a small mass term $H^*\approx E^*+(\hbar^2/m)\boldsymbol{k}^*\cdot\tilde{\boldsymbol{k}}+\lambda(-\tilde{k}_y\sigma_x+\tilde{k}_x\sigma_y)+\Delta^*\sigma_z$ with $\tilde{\boldsymbol{k}}$ being measured with respect to $\boldsymbol{k}^*$, where the Berry curvature is concentrated around $\boldsymbol{k}^*$ as $b\approx\Delta^*\lambda^2/2(\lambda^2\tilde{k}^2+\Delta^{*2})^{3/2}$ and integrated to π if the outer Fermi surface k_F is much larger than the typical scale for the Berry curvature distribution $k_F\gg\Delta^*/\lambda$, which provides the half-quantized plateau feature to the Hall conductance. Of course the contribution from the area away from the anticrossing point $\boldsymbol{k}^*$ will cause deviation from the exact half-quantized value. But our numerical result using the reasonable parameters introduced above strongly suggests that in the cleaning limit we can get a very close half-quantized value with accessible field strength.

Further, our result shows that the Hall conductance has a nearly half-quantized plateau for $n\gtrsim n_0$, but not for $n\lesssim n_0$. Here n_0 is the electron density when chemical potential is at the Dirac point in the absence of magnetic field. The reason is that the kinetic term makes E^* increase as the field increases $E^*=\hbar^2k^{*2}/(2m)$ and E^* is smallest at zero field. Therefore, if $n<n_0$, the chemical potential would not be inside the gap

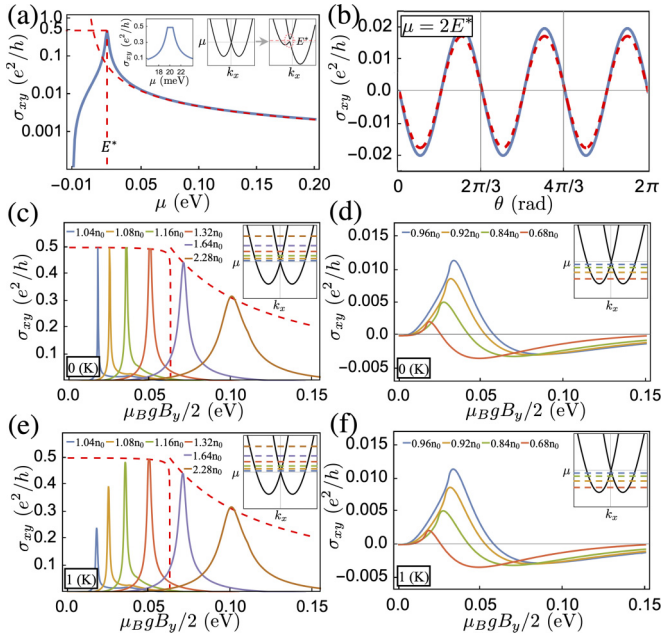

FIG. 1. Intrinsic AHE conductance of nonmagnetic 2DEG with C_{3v} point group symmetry. Numerical values are indicated by solid lines and analytical values are indicated by red dashed lines. The Hamiltonian's parameters are taken as $\hbar^2/(2m) = 2$ eV Å^2, $\lambda = 0.5$ eV Å, $\delta = 0.8$ eV Å^3, $\mu_B g B_x/2 = 0$ eV, and $\mu_B g B_y/2 = 0.05$ eV. Panels (a) and (b) show the conductance versus the chemical potential and the angle of in-plane magnetic field, respectively. In the first inset of (a), the conductance shows a nearly half-quantized plateau around E^*. The evolution of band structure caused by an in-plane magnetic field is shown in the last two insets of (a). The zero temperature Hall conductance versus magnetic field strength with fixed electron density n are shown in (c) for $n \gtrsim n_0$ and (d) for $n \lesssim n_0$, respectively, where n_0 is the electron density when the chemical potential is at the Dirac point in absence of the magnetic field. The insets show the position of the chemical potential in the band structure correspondingly when no magnetic field is applied. In contrast, panels (e) and (f) show the Hall conductance at 1 K temperature.

for any value of the magnetic field. It is worth noting that, in real materials, the warping and Zeeman terms are both relatively much smaller than the Rashba SOC term; then the Hall conductance will be very close to the half-quantized value as indicated by Eq. (5), Figs. 1(c) and 1(e). At the same time, the gap size is tiny and the half-quantized plateau is very narrow, which can only be seen under a very low temperature.

Sb_2Te_3 thin film. The Bi_2Se_3 family of compounds including Bi_2Se_3, Bi_2Te_3, Sb_2Te_3 [24–27], Bi_2Se_2Te, Bi_2Te_2Se, Bi_2Te_2S [28,29], $BiSbTeSe_2$ [30–33], and Sb_2Te_2Se [34,35] are all three-dimensional strong TIs with large bulk band gap predicted by first principle calculations and confirmed by experiments. The crystal structure of these materials is rhombohedral with layered structure. As discussed in [24,36], with symmetry principles and analysis of the atomic orbitals, the model $\boldsymbol{k}\cdot\boldsymbol{p}$ Hamiltonian up to the third order of $\boldsymbol{k}$ around the Γ point can be constructed as follows:

$$H_0 = \epsilon + \mathcal{M}\sigma_z + \mathcal{B}k_z\sigma_y + \mathcal{A}(k_y s_x\sigma_x - k_x s_y\sigma_x) + \mathcal{R}_1 s_z\sigma_x + \mathcal{R}_2\sigma_y + \mathcal{R}_{3x}s_x\sigma_x - \mathcal{R}_{3y}s_y\sigma_x, \quad (6)$$

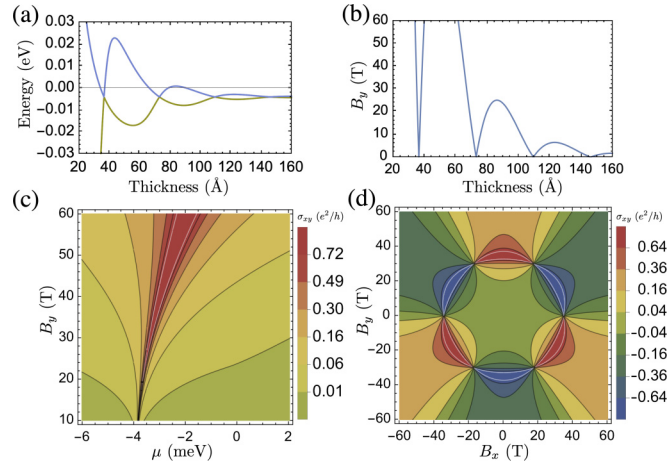

FIG. 2. Subband structure and in-plane AHE of Sb_2Te_3 thin film at the zero temperature limit. (a) Energy levels of subband at Γ point versus film thickness. (b) The minimum in-plane magnetic field strength to achieve QAHE versus thin film thickness, where the field is fixed in the y direction. (c) The AHE conductance versus chemical potential and field strength in the y direction. (d) The AHE conductance versus field strength in both x and y direction, in which the chemical potential is set as -3.2 meV. Both in (c) and (d), the thickness is 110 Å and the Hall conductance reaches the quantized value in the regime enclosed by the white line.

where $\epsilon(\boldsymbol{k}) = C_0 + C_1k_z^2 + C_2k_\parallel^2$, $\mathcal{M}(\boldsymbol{k}) = M_0 + M_1k_z^2 + M_2k_\parallel^2$, $\mathcal{A}(\boldsymbol{k}) = A_0 + A_2k_\parallel^2 + A_3k_z^2$, $\mathcal{B}(\boldsymbol{k}) = B_0 + B_2k_z^2 + B_3k_\parallel^2$, $\mathcal{R}_1(\boldsymbol{k}) = R_1\frac{k_+^3+k_-^3}{2}$, $\mathcal{R}_2(\boldsymbol{k}) = R_2\frac{k_+^3-k_-^3}{2i}$, $\mathcal{R}_{3x} = R_3\frac{(k_+^2+k_-^2)k_z}{2}$, $\mathcal{R}_{3y} = R_3\frac{(k_+^2-k_-^2)k_z}{2i}$, and $k_\parallel^2 = k_x^2 + k_y^2$. And the Zeeman coupling is

$$H_z = \frac{\mu_B}{2}[\tilde{g}_{1z}B_z s_z + \tilde{g}_{1p}(B_x s_x + B_y s_y) + \tilde{g}_{2z}B_z\sigma_z s_z + \tilde{g}_{2p}\sigma_z(B_x s_x + B_y s_y)], \quad (7)$$

where $\tilde{g}_{1z} = (g_{1z} + g_{2z})/2$, $\tilde{g}_{1p} = (g_{1p} + g_{2p})/2$, $\tilde{g}_{2z} = (g_{1z} - g_{2z})/2$, and $\tilde{g}_{2p} = (g_{1p} - g_{2p})/2$. In this work we have calculated all the parameters of this model together with the g factors using the first principle method developed previously by our group [20] for all of the Bi_2Se_3 family of compounds listed above, which are summarized in Table S1 in the SM [22]. Here we have used the generalized gradient approximation and employed the crystal structure parameters given in the corresponding cited references. Among these materials, Bi_2Te_2Se has the largest out of plane g factor being 74.7 and Sb_2Te_3 has the largest in-plane g factor being 19.9. Due to the large in-plane g factor and hexagonal warping term in Sb_2Te_3, we will take it as an example in the following to show that the quantized and nearly half-quantized in-plane AHE can be realized in these materials. The subband Hamiltonian is derived by treating the thin film as a quantum well with infinite potential barrier as discussed in Ref. [37].

As shown in Fig. 2(a), due to quantum confinement, the two lowest energy subbands with opposite parity cross each other repeatedly with the reduction of the film thickness [37–40]. This oscillatory behavior allows us to tune the subband gap by the thickness. When the field is applied in the y direction, which is the bisector between the two neighboring

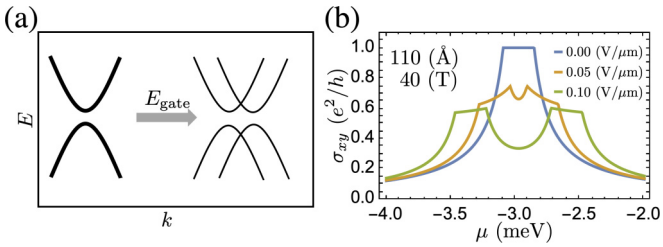

FIG. 3. Evolution of band structure and in-plane AHE conductance induced by gate tuning. Schematic plot (a) shows the evolution of subband structure induced by gate tuning. Panel (b) shows the crossover from quantized to nearly half-quantized in-plane AHE conductance induced by gate tuning for 110 Å thick Sb_2Te_3 thin film at the zero temperature limit.

mirror planes, the required in-plane field strength to realize QAHE also oscillates with the thickness and reaches zeros at those subband level crossing points as shown in Fig. 2(b), and for film thickness around 4 nm, 8 nm, or 11 nm we have the best chance to realize QAHE by in-plane Zeeman effect under a feasible field strength. The in-plane AHE conductance of 110 Å thick thin film at the zero temperature limit as a function of magnetic field strength and chemical potential is shown in Figs. 2(c) and 2(d), in which the Hall conductance reaches the quantized value in the parameter regime enclosed by the white line [22]. The mechanism behind the Chern insulator phases here can still be ascribed to the band inversions at the Γ point. The Zeeman splitting induced by the strong in-plane magnetic field will overcome the gap and invert only a single pair of bands with opposite parity at Γ leading to nonzero Chern number as illustrated in more detail in Ref. [41]. The QAHE discussed here is caused by the in-plane magnetic field through the Zeeman effect and not the in-plane magnetization as proposed in Ref. [16]. In order to realize such an effect, we do not need to dope the thin films with the magnetic ions so the effect can be studied in a wider range of topological insulator thin films without C_{2z} symmetry and with much cleaner samples. The lack of magnetic dopants also provides us with much higher prediction power for the calculations of the real material systems as illustrated in the present paper on the Sb_2Te_3 thin films.

Further, in those systems realizing QAHE, we can introduce a vertical electric field by setting different gate voltage on top and bottom surfaces to break the inversion symmetry, which makes the two Dirac gaps deviate from each other in energy and reduces the point group from D_{3d} to C_{3v}. As shown in Fig. 3(a), the subband structure of the two conduction bands resembles the 2DEG with C_{3v} symmetry given above. Consequently the quantized conductance plateau splits into two nearly half-quantized plateaus at different energy, as shown in Fig. 3(b). In calculations, the electric field is taken into account by adding a diagonal zeE_{gate} term in the quantum well Hamiltonian. And most importantly, unlike the quantized AHE discussed above, we find that half-quantized AHE still can be realized under much feasible field strength. Taking the 60 Å thick thin film as an example [22], the in-plane AHE conductance as a function of chemical potential and field strength are shown in Figs. 4(a) and 4(b), from which we conclude that with strong in-plane magnetic

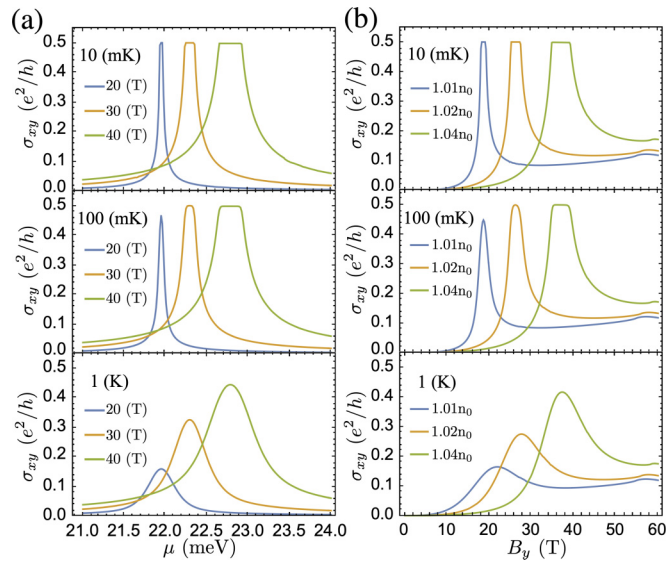

FIG. 4. In-plane nearly half-quantized AHE conductance for 60 Å thick Sb_2Te_3 thin film. Panel (a) is the in-plane AHE conductance versus chemical potential with different field strength and temperature, respectively. Panel (b) is the in-plane AHE conductance versus field strength with different electron density and temperature, respectively. The gate tuning is set as $E_{\text{gate}} = 0.002$ V Å^{-1} and the magnetic field is applied along the y direction.

field $B > 20$ T and low temperature $T < 100$ mK the nearly half-quantized conductance can be observed in such a thin film.

Discussion and conclusion. In this Letter, we propose that the in-plane Zeeman effect induced AHE commonly exists in 2D materials systems with strong SOC but without C_{2z} symmetry. By tuning the field strength and chemical potential, not only quantized but also nearly half-quantized AHE can be realized in these 2D systems, which have not received the attention they deserve in condensed matter physics. Two material examples have been chosen to carry out calculations. The first one is the 2DEG with Rashba type SOC and threefold rotational symmetry. The large in-plane AHE can be realized in such a generic 2D metallic system with the highest in-plane Hall conductance being close to the half-quantized value, which can be approached by tuning both the field strength and the carrier density. The second material example is the Bi_2Se_3 family of thin films, among which we find that Sb_2Te_3 has the largest in-plane Zeeman effect. Then we numerically studied the in-plane Hall effect in Sb_2Te_3 thin film in detail and show that both the quantized and nearly half-quantized AHE conductance can be reached. At last, we would clarify that the nearly half-quantized AHE discussed here is simply due to the existence of a 2D Dirac point in Rashba systems, which can be gapped under in-plane magnetic field. Such a half-quantization has no topological protection and is very different with half-quantization on the surface of topological or axion insulators discussed recently in Refs. [42–44]. Despite the simple physics behind it, such a nearly half-quantized AHE caused by the in-plane magnetic field has been overlooked for a long time and we have the great chance to see it in some realistic 2DEG systems under sufficiently low

temperature, low enough impurity density, and proper carrier density, which may have a stimulating impact on condensed matter and semiconductor experiments.

Acknowledgments X.D. acknowledges financial support from the Hong Kong Research Grants Council (Projects No. GRF16300918 and No. 16309020). H.W. and S.S. acknowledge support from the National Natural Science Foundation (Grants No. 11925408, No. 11921004, and No. 12188101), the Ministry of Science and Technology of China (Grant No. 2018YFA0305700), the Chinese Academy of Sciences (Grant No. XDB33000000), the K. C. Wong Education Foundation (Grant No. GJTD-2018-01), and the Informatization Plan of Chinese Academy of Sciences (Grant No. CAS-WX2021SF-0102).

[1] N. Nagaosa, J. Sinova, S. Onoda, A. H. MacDonald, and N. P. Ong, Anomalous Hall effect, Rev. Mod. Phys. **82**, 1539 (2010).

[2] R. Karplus and J. M. Luttinger, Hall effect in ferromagnetics, Phys. Rev. **95**, 1154 (1954).

[3] Y. Yao, L. Kleinman, A. H. MacDonald, J. Sinova, T. Jungwirth, D.-s. Wang, E. Wang, and Q. Niu, First Principles Calculation of Anomalous Hall Conductivity in Ferromagnetic bcc Fe, Phys. Rev. Lett. **92**, 037204 (2004).

[4] X. Wang, J. R. Yates, I. Souza, and D. Vanderbilt, *Ab initio* calculation of the anomalous Hall conductivity by Wannier interpolation, Phys. Rev. B **74**, 195118 (2006).

[5] X. Wang, D. Vanderbilt, J. R. Yates, and I. Souza, Fermi-surface calculation of the anomalous Hall conductivity, Phys. Rev. B **76**, 195109 (2007).

[6] H. Kontani, T. Tanaka, and K. Yamada, Intrinsic anomalous Hall effect in ferromagnetic metals studied by the multi-*d*-orbital tight-binding model, Phys. Rev. B **75**, 184416 (2007).

[7] C.-X. Liu, S.-C. Zhang, and X.-L. Qi, The quantum anomalous Hall effect: Theory and experiment, Annu. Rev. Condens. Matter Phys. **7**, 301 (2016).

[8] F. D. M. Haldane, Model for a Quantum Hall Effect without Landau Levels: Condensed-Matter Realization of the "Parity Anomaly", Phys. Rev. Lett. **61**, 2015 (1988).

[9] D. J. Thouless, M. Kohmoto, M. P. Nightingale, and M. den Nijs, Quantized Hall Conductance in a Two-Dimensional Periodic Potential, Phys. Rev. Lett. **49**, 405 (1982).

[10] S. Sun, Z. Song, H. Weng, and X. Dai, Topological metals induced by the Zeeman effect, Phys. Rev. B **101**, 125118 (2020).

[11] Z. Sun, Z. Cao, J. Cui, C. Zhu, D. Ma, H. Wang, W. Zhuo, Z. Cheng, Z. Wang, X. Wan, and X. Chen, Large zeeman splitting induced anomalous hall effect in $ZrTe_5$, npj Quantum Mater. **5**, 36 (2020).

[12] J. Ahn and B.-J. Yang, Unconventional Topological Phase Transition in Two-Dimensional Systems with Space-Time Inversion Symmetry, Phys. Rev. Lett. **118**, 156401 (2017).

[13] C. Fang and L. Fu, New classes of three-dimensional topological crystalline insulators: Nonsymmorphic and magnetic, Phys. Rev. B **91**, 161105(R) (2015).

[14] L. M. Roth, B. Lax, and S. Zwerdling, Theory of optical magneto-absorption effects in semiconductors, Phys. Rev. **114**, 90 (1959).

[15] R. Winkler, *Spin-Orbit Coupling Effects in Two-Dimensional Electron and Hole Systems* (Springer, New York, 2003), Vol. 191.

[16] X. Liu, H.-C. Hsu, and C.-X. Liu, In-Plane Magnetization-Induced Quantum Anomalous Hall Effect, Phys. Rev. Lett. **111**, 086802 (2013).

[17] Y. A. Bychkov and É. I. Rashba, Properties of a 2d electron gas with lifted spectral degeneracy, JETP Lett. **39**, 78 (1984).

[18] A. Manchon, H. C. Koo, J. Nitta, S. M. Frolov, and R. A. Duine, New perspectives for rashba spin–orbit coupling, Nat. Mater. **14**, 871 (2015).

[19] L. Fu, Hexagonal Warping Effects in the Surface States of the Topological Insulator Bi_2Te_3, Phys. Rev. Lett. **103**, 266801 (2009).

[20] Z. Song, S. Sun, Y. Xu, S. Nie, H. Weng, Z. Fang, and X. Dai, First principle calculation of the effective Zeeman's couplings in topological materials, *Memorial Volume for Shoucheng Zhang* (World Scientific, 2022), pp. 263–281.

[21] X.-L. Qi, Y.-S. Wu, and S.-C. Zhang, Topological quantization of the spin Hall effect in two-dimensional paramagnetic semiconductors, Phys. Rev. B **74**, 085308 (2006).

[22] See Supplemental Material at http://link.aps.org/supplemental/10.1103/PhysRevB.106.L241105 for (I) parameters of $\boldsymbol{k}\cdot\boldsymbol{p}$ Hamiltonian and g factor for Bi_2Se_3 family, (II) analytical derivation for the in-plane AHE in quasi-2D metals with C_{3v} symmetry, (III) the quantized in-plane AHE plateau, (IV) the evolution of band structure induced by gate tuning and in-plane magnetic field, and (V) the real-space distribution of wave function and half-quantized AHE conductance, which includes [21,26,29,34,45–47].

[23] For BiTeI [48], $\lambda = 3.8\text{eV Å}$ and $m = 0.1m_e$ (m_e is the free electron mass). For the surface states of Bi_2Se_3 [24,49], $\lambda = 3.3\text{eV Å}$ and $m = 0.07m_e$. Therefore, by using typical parameters $\lambda \sim 3$ eV Å, $m \sim 0.1m_e$, the γ is estimated to be $\gamma \sim 0.12 \ll 1$ even for huge magnetic field $B_\parallel \sim 50\text{T}$ and g factor $g \sim 10$.

[24] H. Zhang, C.-X. Liu, X.-L. Qi, X. Dai, Z. Fang, and S.-C. Zhang, Topological insulators in Bi_2Se_3, Bi_2Te_3 and Sb_2Te_3 with a single Dirac cone on the surface, Nat. Phys. **5**, 438 (2009).

[25] Y. Xia, D. Qian, D. Hsieh, L. Wray, A. Pal, H. Lin, A. Bansil, D. Grauer, Y. S. Hor, R. J. Cava, and M. Z. Hasan, Observation of a large-gap topological-insulator class with a single Dirac cone on the surface, Nat. Phys. **5**, 398 (2009).

[26] W. Zhang, R. Yu, H.-J. Zhang, X. Dai, and Z. Fang, First-principles studies of the three-dimensional strong topological insulators Bi_2Te_3, Bi_2Se_3 and Sb_2Te_3, New J. Phys. **12**, 065013 (2010).

[27] J. G. Analytis, R. D. McDonald, S. C. Riggs, J.-H. Chu, G. S. Boebinger, and I. R. Fisher, Two-dimensional surface state in the quantum limit of a topological insulator, Nat. Phys. **6**, 960 (2010).

[28] Z. Ren, A. A. Taskin, S. Sasaki, K. Segawa, and Y. Ando, Large bulk resistivity and surface quantum oscillations in the

topological insulator Bi_2Te_2Se, Phys. Rev. B **82**, 241306(R) (2010).

[29] L.-L. Wang and D. D. Johnson, Ternary tetradymite compounds as topological insulators, Phys. Rev. B **83**, 241309(R) (2011).

[30] T. Arakane, T. Sato, S. Souma, K. Kosaka, K. Nakayama, M. Komatsu, T. Takahashi, Z. Ren, K. Segawa, and Y. Ando, Tunable Dirac cone in the topological insulator $Bi_{2-x}Sb_xTe_{3-y}Se_y$, Nat. Commun. **3**, 636 (2012).

[31] B. Xia, P. Ren, A. Sulaev, P. Liu, S.-Q. Shen, and L. Wang, Indications of surface-dominated transport in single crystalline nanoflake devices of topological insulator $Bi_{1.5}Sb_{0.5}Te_{1.8}Se_{1.2}$, Phys. Rev. B **87**, 085442 (2013).

[32] K. Segawa, Z. Ren, S. Sasaki, T. Tsuda, S. Kuwabata, and Y. Ando, Ambipolar transport in bulk crystals of a topological insulator by gating with ionic liquid, Phys. Rev. B **86**, 075306 (2012).

[33] Y. Xu, I. Miotkowski, C. Liu, J. Tian, H. Nam, N. Alidoust, J. Hu, C.-K. Shih, M. Z. Hasan, and Y. P. Chen, Observation of topological surface state quantum Hall effect in an intrinsic three-dimensional topological insulator, Nat. Phys. **10**, 956 (2014).

[34] T. L. Anderson and H. B. Krause, Refinement of the Sb_2Te_3 and Sb_2Te_2Se structures and their relationship to nonstoichiometric $Sb_2Te_{3-y}Se_y$ compounds, Acta Crystallogr. B: Struct. Sci. **30**, 1307 (1974).

[35] C.-K. Lee, C.-M. Cheng, S.-C. Weng, W.-C. Chen, K.-D. Tsuei, S.-H. Yu, M. M.-C. Chou, C.-W. Chang, L.-W. Tu, H.-D. Yang, C.-W. Luo, and M. M. Gospodinov, Robustness of a topologically protected surface state in a Sb_2Te_2Se single crystal, Sci. Rep. **6**, 36538 (2016).

[36] C.-X. Liu, X.-L. Qi, H.-J. Zhang, X. Dai, Z. Fang, and S.-C. Zhang, Model Hamiltonian for topological insulators, Phys. Rev. B **82**, 045122 (2010).

[37] C.-X. Liu, H.-J. Zhang, B. Yan, X.-L. Qi, T. Frauenheim, X. Dai, Z. Fang, and S.-C. Zhang, Oscillatory crossover from two-dimensional to three-dimensional topological insulators, Phys. Rev. B **81**, 041307(R) (2010).

[38] H.-Z. Lu, W.-Y. Shan, W. Yao, Q. Niu, and S.-Q. Shen, Massive Dirac fermions and spin physics in an ultrathin film of topological insulator, Phys. Rev. B **81**, 115407 (2010).

[39] J. Linder, T. Yokoyama, and A. Sudbø, Anomalous finite size effects on surface states in the topological insulator Bi_2Se_3, Phys. Rev. B **80**, 205401 (2009).

[40] W.-Y. Shan, H.-Z. Lu, and S.-Q. Shen, Effective continuous model for surface states and thin films of three-dimensional topological insulators, New J. Phys. **12**, 043048 (2010).

[41] R. Yu, W. Zhang, H.-J. Zhang, S.-C. Zhang, X. Dai, and Z. Fang, Quantized anomalous Hall effect in magnetic topological insulators, Science **329**, 61 (2010).

[42] M. Mogi, Y. Okamura, M. Kawamura, R. Yoshimi, K. Yasuda, A. Tsukazaki, K. S. Takahashi, T. Morimoto, N. Nagaosa, M. Kawasaki, Y. Takahashi, and Y. Tokura, Experimental signature of the parity anomaly in a semi-magnetic topological insulator, Nat. Phys. **18**, 390 (2022).

[43] J.-Y. Zou, B. Fu, H.-W. Wang, Z.-A. Hu, and S.-Q. Shen, Half-quantized Hall effect and power law decay of edge-current distribution, Phys. Rev. B **105**, L201106 (2022).

[44] B. Fu, J.-Y. Zou, Z.-A. Hu, H.-W. Wang, and S.-Q. Shen, Quantum anomalous semimetals, arXiv:2203.00933.

[45] Z. Ren, A. A. Taskin, S. Sasaki, K. Segawa, and Y. Ando, Optimizing $Bi_{2-x}Sb_xTe_{3-y}Se_y$ solid solutions to approach the intrinsic topological insulator regime, Phys. Rev. B **84**, 165311 (2011).

[46] M. Gu, J. Li, H. Sun, Y. Zhao, C. Liu, J. Liu, H. Lu, and Q. Liu, Spectral signatures of the surface anomalous Hall effect in magnetic axion insulators, Nat. Commun. **12**, 3524 (2021).

[47] N. Varnava and D. Vanderbilt, Surfaces of axion insulators, Phys. Rev. B **98**, 245117 (2018).

[48] K. Ishizaka, M. S. Bahramy, H. Murakawa, M. Sakano, T. Shimojima, T. Sonobe, K. Koizumi, S. Shin, H. Miyahara, A. Kimura, K. Miyamoto, T. Okuda, H. Namatame, M. Taniguchi, R. Arita, N. Nagaosa, K. Kobayashi, Y. Murakami, R. Kumai, Y. Kaneko *et al.*, Giant rashba-type spin splitting in bulk bitei, Nat. Mater. **10**, 521 (2011).

[49] L. He, F. Xiu, X. Yu, M. Teague, W. Jiang, Y. Fan, X. Kou, M. Lang, Y. Wang, G. Huang, N.-C. Yeh, and K. L. Wang, Surface-dominated conduction in a 6 nm thick bi2se3 thin film, Nano Lett. **12**, 1486 (2012).